Dual-scale robotic solution for middle ear surgery

Jae-Hun So, Brahim Tamadazte, Naresh Marturi, Jérôme Szewczyk

Dual-scale robotic solution for middle ear surgery

Jae-Hun So[1], Brahim Tamadazte[1], Naresh Marturi[2], and Jérôme Szewczyk[1].

Abstract— **This paper deals with the control of a redundant robotic system for middle ear surgery (i.e., cholesteatoma tissues removal). The targeted robotic system is a macro-micro-scale robot composed of a redundant seven degrees of freedom (DoFs) on which is attached a two DoFs robotized flexible fiberscope. Two different control architectures are proposed to achieve a defined surgical procedure to remove the pathological tissue inside the middle ear cavity. The first proposed control mode is based on the position-based tele-operation of the entire system using a joystick (Phantom Omni) as a master arm. The second one combines comanipulation of the seven DoFs robotic arm using an embedded force/torque sensor and an end-frame tele-operation of the remaining two DoFs fiberscope using a lab-made in-hand joystick. Experimental validation is performed to evaluate and compare the performance of both developed control schemes. The obtained results using the lab-made platform and the proposed controllers are discussed.**

I. INTRODUCTION

Robotized Minimally Invasive Surgery (MIS) is gaining more and more importance through increasing accuracy in control of robotic tools [1]. The use of robotized MIS to smaller workspaces (millimetric scale) is also a significant trend. Thus, otorhinolaryngology surgery would greatly benefit from a robotic assistance as this surgery suffers lack of vision and shows a very limited workspace. This is particularly true when dealing with middle ear interventions as in the case of mechanical ablation cholesteatoma tissues.

From a clinical point of view, it is stated that cholesteatoma disease is related to be a ventilation problem where dead skin cells cannot be ejected from the tympani. This pile of tumorous tissue expands throughout the middle ear also filling the cavity space. The increasing volume of the cholesteatoma tissue will start eroding functional organs and outlining bone, the mastoid, etc. Consequently, the results of this disease are hearing loss, dizziness and at severe condition, a partial facial palsy, etc. It is reported that one case per 10,000 citizens occurs every year in European countries [2]. The only treatment of cholesteatoma is to mechanically remove the major portion of the pathological tissue and to perform a laser ablation for the residual cholesteatoma cells [3], [4].

Basically, there are two surgical protocols for treating cholesteatoma. The first one uses the ear canal to reach the middle ear cavity with small rigid instruments [5]. However, this protocol is not widely used as it can only be achieved at the early stage of cholesteatoma development. The second surgical procedure is based on performing a mastoidectomy, which consists of a large incision hole (20-25mm of diameter) to the middle ear cavity, so that the physician has a direct access and vision of the middle ear cavity to mechanically remove the pathological tissues with adapted surgical tools [4]. This procedure has become a standard for a long time despite several limitations: complex procedure, invasiveness, high failure rate (20%-25% of procedures require re-operation), and difficulty in exhaustive removal of all the pathological tissues [6], [7]. The current surgical protocol, in addition to being invasive, requires a high know-how of the surgeon. This may partially explain the high failure rate of this type of surgery, caused by the residual cholesteatoma cells that remain after the intervention [8]. Hence, there is a high demand for improvement of current surgical procedures towards less invasive approaches by reducing the incision hole, as well as improving the efficiency of the ablation of infected pathological tissues, and then to avoid repeated surgery.

Among the possibilities for improvement, robotic solutions to improve the procedure of tissue removal include robotic holders, innovative surgical tools, advanced imaging systems, as well as advanced control schemes to ensure a precise and safe infected tissue resection or ablation [9]–[13]. Several robots have been designed for middle ear surgery to enhance accuracy, dexterity and ergonomic to the physician. They are mainly dedicated to cochlear implantation [14], tympanic membrane grafts or ossicular chain replacement [15], [16] which requires high accuracy and reproducibility in different patients. However, all these solutions are based on rigid tools and does not include any dexterous instrument for intracorporeal fine movement execution. Other works highlight the feasibility of robot-assisted ear surgery such as robot-assisted mastoidectomy [17] and tool-guidance [16]. However, these approaches are not suited for cholesteatoma surgery which requires high accuracy and dexterity due to limited workspace and the presence of the ossicles and facial nerve within the middle ear cavity.

This paper investigates two main aspects of the targeted robotic system, which have never been investigated for middle ear surgery. Firstly, we developed an original and redundant dual-scale robotic system teleoperated using a specific embedded 2 DoFs joystick attached to the 7 DoFs robotic arm. Secondly, we have designed controllers ensuring the control of the macro-micro system in order to achieve accurate positioning tasks in a constrained environment (e.g., middle ear cavity):

- an end-frame tele-operation of the whole kinematic structure with an intuitive and transparent management

This work has been supported by French ANR μRoCS Project no ANR-17-CE19-0005-04. [1]Sorbonne Université, CNRS UMR 7222, INSERM U1150, ISIR, F-75005, Paris, France. [2]Extreme Robotics Laboratory, University of Birmingham, Birmingham, U.K. so@isir.upmc.fr.

of the fulcrum effect;
- a combination of a comanipulation method for the macro-scale robot and of an in-hand tele-operation of the micro-scale tool.

Both the developed dual-scale robotic system and the control schemes were evaluated individually and compared through scenarios that mimic the task of pointing out residual cholesteatoma cells with a surgical laser.

The rest of this paper is organized as follows. Section II deals with the design of the macro-micro-robotic system integrating a flexible endoscopic tool, when Section III discusses the kinematics modelling of the whole robotic system. The integration of the control interface is discussed in Section IV and the experimental evaluation of the proposed materials and methods is reported in Section V.

II. MACRO-MICRO ROBOTIC SYSTEM

The first contribution of this work concerns the development of a macro-micro robotic system (Fig. 1) dedicated to middle ear interventions. It consists of a Panda robot arm (macro-scale system) on which is fixed a flexible fiberscope (micro-scale tool) actuated with a tendon-driven continuum mechanism.

A. Design of the Macro-Micro Manipulator System

The macro-micro robotic system was designed to obtain a redundant kinematic structure that operates in a limited and constrained space (middle ear cavity). Actually, the total number of DoFs has been chosen to efficiently control the system end-effector motion while satisfying kinematic constraints at the entrance point of the middle ear. The macro-scale system is a 7 DoFs Panda arm from Franka Emika (Fig. 1) equipped with a Force/Torque (F/T) sensor (ATI MINI-40) attached at its end-effector part. Its redundancy allows an internal motion for safer use of the robot. The flexible micro-scale tool, which consists of a fiberscope from Karl Storz (11292AD1) with two actuated DoFs, is fixed at the Panda end-effector. The flexible tool is namely a $\pm 90°$ flexion and a 50 mm translation (see right side of Fig. 1). It is mounted in such a way that its straight configuration coincides with the z-axis of the last joint of the Panda robot.

The micro-tool transmission is assembled in two parts. The flexion actuation unit is located at the proximal end of the fiberscope (handle) and is positioned outside the system due to its unsuitable payload. The flexion is produced by a linear shaft coupled to the original fiberscope handle through a bilateral punctual contact. This linear shaft is actuated by an linear servomotor from Actuonix (L16-100-35-12-P) which also provides the measure of the fiberscope flexion angle (Fig. 1). As for the translational actuation of the fiberscope, a linear actuator is embedded in a chassis directly mounted on the Panda end-effector. A servomotor controls the position of the linear joint (L16-50-35-6-R). This 2 DoFs actuation system is controlled through a low-level position controller implemented on an Arduino Mega micro-controller board and Actuonix Servo Controller. A designed hand-grip for

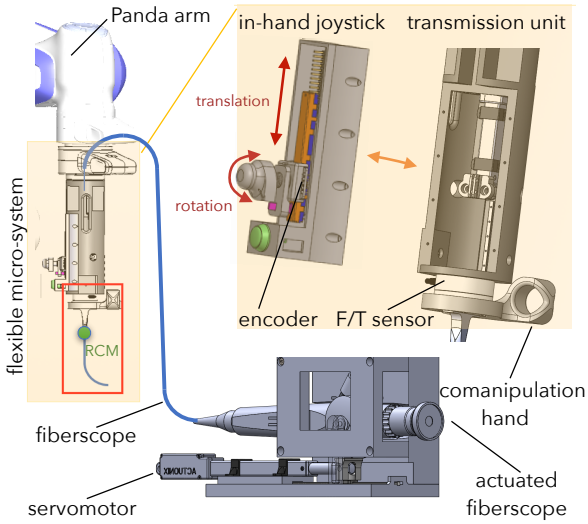

Fig. 1. Macro-micro-scale robotic system with detailed parts description.

comanipulation mode is attached at the base of the micro-tool chassis as depicted in Fig. 1.

B. Design of the Control Architecture

The robotic control system is implemented on a server PC using Robot Operating System (ROS), with Ubuntu 16.04 LTS. Furthermore, the end-frame tele-operation of the macro-micro-scale robot is performed using a Sensable Phantom Omni as a master arm.

As for the comanipulation mode, a F/T sensor is attached between the robot end-effector and the micro-scale tool so that the macro-robot terminal body can be handled by the user without any constraints. Meanwhile, the micro-tool which enters inside the middle ear cavity is controlled using a small size 2 DoFs lab-made joystick attached to the Panda robot end-effector. It is embedded on the micro-tool chassis near the comanipulation handle and has the same motion features as the fiberscope, i.e., translation and flexion.

The fact that this joystick is mounted on the micro-tool chassis and is structurally aligned with the micro-tool axis avoid any mental registration by the surgeon during the task [22]. A rotary encoder mounted on a linear potentiometer measures both the value of the desired flexion angle and the desired position of the prismatic joint, respectively. In this work, a BOURNS absolute 128 positions rotary encoder (EAW0J-B24-AE0128L) and an Alps Alpine (RS6011Y1600Q) linear potentiometer are used.

III. KINEMATIC MODELING

The obtained macro-micro-scale manipulator is then a redundant kinematic chain of 9 DoFs (i.e., 7 DoFs of the Panda arm plus 2 DoFs of the flexible micro-scale tool). In the following we discuss the kinematic modelling of the whole system.

A. Mapping between Joint Space and Task Space

First, we derive the forward kinematic model establishing a mathematical relation between the robotic system joint

variables and the end-effector frame configuration with respect to the robot base frame $\mathcal{R}_0$. This model can be split into two parts corresponding to the Panda arm and the micro-scale subsystem. Each sub-model is identified through a transformation matrix linking the last and the first frames of the corresponding chain.

Actually, the mapping between the macro-scale subsystem joint values and its operational configuration ($\mathcal{R}_7$) is obtained via the modified Denavit-Hartenberg (D-H) parameters which are expressed as follows:

$$ {}^{i-1}\mathbf{T}_i = \begin{bmatrix} c_{\theta_i} & -s_{\theta_i} & 0 & a_{i-1} \\ s_{\theta_i}c_{\alpha_{i-1}} & c_{\theta_i}c_{\alpha_{i-1}} & -s_{a_{i-1}} & -d_i s_{a_{i-1}} \\ -s_{\theta_i}c_{\alpha_{i-1}} & c_{\theta_i}s_{\alpha_{i-1}} & c_{a_{i-1}} & d_i c_{a_{i-1}} \\ 0 & 0 & 0 & 1 \end{bmatrix} \quad (1) $$

where i is the index of the i-th actuator for $i = 1, 2, \cdots, 7$, $s_{\theta_i} = \sin(\theta_i), c_{\theta_i} = \cos(\theta_i)$, and d_i, a_i, θ_i, α_i are the modified D-H parameters as shown in Fig. 2(a). Intuitively, the kinematic model of the macro-scale system is obtained as follows:

$$ {}^0\mathbf{T}_7 = {}^0\mathbf{T}_1 {}^1\mathbf{T}_2 {}^2\mathbf{T}_3 {}^3\mathbf{T}_4 {}^4\mathbf{T}_5 {}^5\mathbf{T}_6 {}^6\mathbf{T}_7 \quad (2) $$

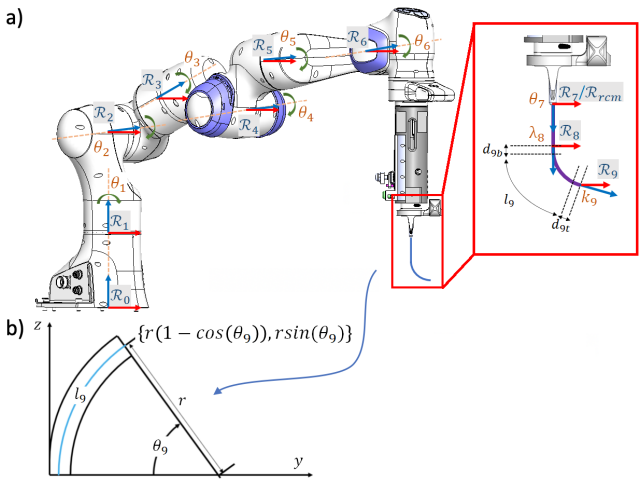

Fig. 2. Kinematic diagram of a) the whole robotic system and b) the flexible part.

Concerning the micro-tool part, the first actuated motion is a translation. The distance between $\mathcal{R}_7$ and $\mathcal{R}_8$ along the z_7 axis varies as the distance λ_8. This leads to a transformation matrix ${}^7\mathbf{T}_8$ expressed as follows:

$$ {}^7\mathbf{T}_8 = \begin{bmatrix} 1 & 0 & 0 & 0 \\ 0 & 1 & 0 & 0 \\ 0 & 0 & 1 & \lambda_8 \\ 0 & 0 & 0 & 1 \end{bmatrix} \quad (3) $$

The second actuation is a flexion of the tool-tip. The constant curvature model [18], [19] is used here to compute the transformation matrix for flexion between $\mathcal{R}_8$ and $\mathcal{R}_9$. For that, the fiberscope terminal body is divided in three parts: 1) a rigid part d_{9b}, 2) a flexible bending mechanism with l_9 and 3) another rigid part at the tool-tip d_{9t} as shown in Fig. 2(a). According to Fig. 2(b), the flexion position can be computed as $y = r * (1 - \cos(\theta_9))$ and $z = r * \sin(\theta_9)$ where $r = l_9/\theta_9$ is the radius of the arc made by the flexion and θ_9 the angular position, and leads to the following expression:

$$ \begin{pmatrix} x_9 \\ y_9 \\ z_9 \end{pmatrix} = \begin{pmatrix} 0 \\ \frac{l_9}{\theta_9}\left(1 - \cos(\theta_9)\right) \\ \frac{l_9}{\theta_9}\left(\sin\left(\theta_9\right)\right) \end{pmatrix} \quad (4) $$

By defining a new joint variable k_9 which gives the flexion angle between z_8 and z_9, the value of k_9 is computed using $k_9 = \frac{\theta_9}{l_9}$. Thus, the transformation matrix ${}^8\mathbf{T}_9$ function of the new variable k_9 is expressed by:

$$ {}^8\mathbf{T}_9 = \begin{bmatrix} 1 & 0 & 0 & 0 \\ 0 & c(k_9 l_9) & -s(k_9 l_9) & d_{9t}\ s(k_9 l_9) - (1 - c(k_9 l_9))/k_9 \\ 0 & s(k_9 l_9) & c(k_9 l_9) & d_{9b} + d_{9t}\ c(k_9 l_9) + s(k_9 l_9)/k_9 \\ 0 & 0 & 0 & 1 \end{bmatrix} \quad (5) $$

As result, the transformation matrix from $\mathcal{R}_0$ to $\mathcal{R}_9$ is obtained by the product of equations (2), (3) and (5) giving the following expression:

$$ {}^0\mathbf{T}_9 = {}^0\mathbf{T}_7 {}^7\mathbf{T}_8 {}^8\mathbf{T}_9 = \begin{bmatrix} {}^0\mathbf{R}_9 & {}^0\mathbf{t}_9 \\ 0 & 1 \end{bmatrix} \quad (6) $$

here, ${}^0\mathbf{R}_9 \in \mathbb{R}^{3\times3}$ and ${}^0\mathbf{t}_9 \in \mathbb{R}^3$ are respectively the rotation matrix and translation vector of the tool-tip frame $\mathcal{R}_9$ with respect to the base frame $\mathcal{R}_0$. The velocity-level kinematic mapping between the joint configuration space and the task space can be obtained by:

$$ {}^0\dot{\mathbf{x}} = \mathbf{J}\ \dot{\mathbf{q}} \quad (7) $$

where ${}^0\dot{\mathbf{x}} = [{}^0\mathbf{v}^\intercal, {}^0\omega^\intercal]^\intercal \in \mathbb{R}^6$ represents the linear and angular velocities of the tool-tip with respect to the base frame $\mathcal{R}_0$ and $\dot{\mathbf{q}} = [\dot{\theta}_1, \dot{\theta}_2, \cdots, \dot{\theta}_7, \dot{\lambda}_8, \dot{k}_9]^\intercal \in \mathbb{R}^9$ is the joint-velocity vector; and $\mathbf{J} \in \mathbb{R}^{6\times9}$ is the robot Jacobian matrix which can be calculated using (6).

B. Remote Center of Motion Simplification

In order to tackle the kinematic constraints entailed by the narrow access through the performed mastoid hole, we impose a virtual remote center of motion (RCM) to the robot at the position of the insertion point into the mastoid linked to the frame $\mathcal{R}_{rcm}$ (Fig. 2)(a). Concretely, the point O_{RCM}, located on the Z_7 axis where the flexible fiberscope emerges from the chassis, is imposed to coincide with this insertion point and to be motionless.

Therefore, considering the virtual RCM, the fiberscope end-frame configuration is now uniquely controlled by the three rotations of the Panda's end-effector at this point and by the two DoFs of the micro-tool. Consequently, we defined a reduced set of joint variables including the $\mathcal{R}_7$ Roll-Pitch-Yaw (RPY) angles with respect to $\mathcal{R}_{rcm}$ plus the micro-tool motions λ_8 and k_9. The corresponding simplified kinematic model is expressed thanks to the transformation ${}^{rcm}\mathbf{T}_7$ defined by:

$$ {}^{rcm}\mathbf{T}_7 = \begin{bmatrix} c_\beta c_\gamma & c_\gamma s_\alpha s_\beta - c_\alpha s_\gamma & s_\alpha s_\gamma + c_\alpha c_\gamma s_\beta & 0 \\ c_\beta s_\gamma & c_\alpha c_\gamma + s_\alpha s_\beta s_\gamma & c_\alpha s_\beta s_\gamma - c_\gamma s_\alpha & 0 \\ -s_\beta & c_\beta s_\alpha & c_\alpha c_\beta & 0 \\ 0 & 0 & 0 & 1 \end{bmatrix} \quad (8) $$

where α, β and γ are the three rotations at the $\mathcal{R}_{rcm}$, and $s_i = \sin(i)$, $c_i = \cos(i)$. The transformation matrix from $\mathcal{R}_{rcm}$ to $\mathcal{R}_9$ and the corresponding mapping equation between the joint and task space velocities are thus:

$$^{rcm}\mathbf{T}_9^* = {}^{rcm}\mathbf{T}_7\,{}^7\mathbf{T}_8\,{}^8\mathbf{T}_9 = \begin{bmatrix} {}^{rcm}\mathbf{R}_9 & {}^{rcm}\mathbf{t}_9 \\ 0 & 1 \end{bmatrix} \quad (9)$$

with ${}^{rcm}\mathbf{R}_9 \in \mathbb{R}^{3\times3}$ and ${}^{rcm}\mathbf{t}_9 \in \mathbb{R}^3$ are respectively the rotation matrix and translation vector of the tool-tip frame $\mathcal{R}_9$ according to the RCM frame $\mathcal{R}_{rcm}$. Thereby, the velocity-level kinematic mapping between the joint space and the task space can be also obtained by:

$$^{rcm}\dot{\mathbf{x}} = \mathbf{J}^*\ \dot{\mathbf{q}}^* \quad (10)$$

with $\dot{\mathbf{q}}^* = [\dot{\theta}_\alpha, \dot{\theta}_\beta, \dot{\theta}_\gamma, \dot{\lambda}_8, \dot{k}_9]^\intercal$, the joint space velocity vector and ${}^{rcm}\dot{\mathbf{x}} \in \mathbb{R}^6$, the task space velocity vector expressed in $\mathcal{R}_{rcm}$, and $\mathbf{J}^* \in \mathbb{R}^{6\times5}$ the Jacobian matrix of the simplified model.

As the origins of $\mathcal{R}_7$ and $\mathcal{R}_{rcm}$ always coincide, the operational velocity vector of the macro-scale robot can be expressed as $\dot{\mathbf{x}}_7 = [0_{3\times1}, \dot{\theta}_\alpha, \dot{\theta}_\beta, \dot{\theta}_\gamma]^\intercal$ with $\dot{\theta}_\alpha, \dot{\theta}_\beta, \dot{\theta}_\gamma$ from $\dot{\mathbf{q}}^*$. Also, the mapping between the macro-scale robot joint and task spaces is formulated thanks to:

$$^{\mathbf{0}}\dot{\mathbf{x}}_7 = \mathbf{J}_7\ \dot{\mathbf{q}}_7 \quad (11)$$

with $\dot{\mathbf{q}}_\mathbf{7} = [\dot{\theta}_1, \dot{\theta}_2, \cdots, \dot{\theta}_7]^\intercal$ the joint-space velocity vectors and $\mathbf{J}_7 \in \mathbb{R}^{6\times7}$, the Jacobian matrix for the motion of the macro-scale robot expressed in the RCM point. Thanks to this simplified two parts kinematic model, the computation process is much easier than applying the global nine DoFs Jacobian matrix of (7).

IV. CONTROL METHODOLOGIES

In order to control the redundant robotic system, two different control schemes were developed, evaluated, and compared using a scenario simulating the laser ablation of residual cholesteatoma inside the middle ear cavity. One is an intuitive end-frame tele-operation, when the second consists of the combination of macro-comanipulation and micro-tele-operation approach in which the Panda robot is controlled by comanipulation and the micro-scale tool by the embedded 2 DoFs joystick.

A. End-frame Tele-operation

Tele-operation is widely used in different contexts and applications, namely in industrial [21] and medical robotics [20]. In our investigation which deals with minimally invasive surgery of cholesteatoma, the surgeon directly controls the system end-effector by a master arm, while the RCM kinematic constraint is automatically fulfilled by the controller exploiting the redundancies in the developed kinematic chain. The advantage of using such an approach lies in the direct mapping between the master arm and the end-effector motion while the RCM constraint remains transparent for the user. However, this approach requires a precise registration between the environment and the robot base frame along with an accurate positioning of the kinematic constraint location.

In order to control the tool-tip motion whose pose and velocities are primarily defined in the RCM frame $\mathcal{R}_{rcm}$ according to (9) and (10), the control variables have to be shifted to the micro-tool tip frame $\mathcal{R}_9$ using a new Jacobian matrix $\mathbf{J}_{tip} \in \mathbb{R}^{6\times5}$ expressed as follows:

$$\mathbf{J}_{tip} = \begin{bmatrix} \mathbf{I}_{3\times3} & 0 \\ 0 & {}^{rcm}\mathbf{R}_9 \end{bmatrix}_{6\times6} \mathbf{J}^* \quad (12)$$

Because $\mathbf{J}_{tip}$ is a rectangular matrix with only five inputs (joint variables) and six outputs (task space variables), one component of the task space has to remain uncontrolled. As the tool-tip rotation around its own axis z_9 is not important for a pointing task, this corresponding DoF can remain uncontrolled without affecting the task execution.

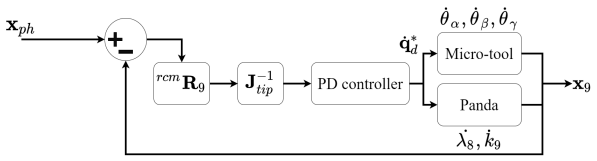

Fig. 3. Control loop of the tele-operation.

The resulting end-frame tele-operation scheme is depicted in Fig. 3. As we can see, the error at task-space level between the master-arm (Phantom Omni) configuration $\mathbf{x}_{ph}$ and the tool-tip configuration $\mathbf{x}_9$ is first converted at joint space level using the inverse of the reduced Jacobian matrix issued from $\mathbf{J}_{tip}$. Then, a Proportional Derivative (PD) controller is applied to obtain the desired joint velocities $\dot{\mathbf{q}}_d^*$ that serve as inputs to the Panda robot and the micro-scale tool unit.

B. Macro-comanipulation and Micro-tele-operation

The second control scheme is based on a dual loop control integrating macro-comanipulation and micro-tele-operation (MCMT). It is separated into two control layers (as can be seen in Fig. 4) working in parallel: a control law for the macro-scale extra-corporeal part and another for the micro intra-corporeal one. Note that this control approach does not require any registration nor kinematic constraint modelling.

The macro extra-corporeal part is directly guided by the user in a comanipulation manner using an admittance control scheme through measurement of the F/T sensor of the wrench $\mathbf{f}_s = [f_s^\intercal, \tau_s^\intercal]^\intercal \in \mathbb{R}^6$ he/she applies at the grip handle. As $\mathbf{f}_s$ is applied on $\mathcal{R}_{rcm}$, the converted vector $\mathbf{f}_{ext}$ with respect to $\mathcal{R}_0$ can be computed as:

$$\mathbf{f}_{ext} = ({}^0\mathbf{R}_{rcm})^\intercal\ \mathbf{f}_s \quad (13)$$

by using the rotation matrix ${}^0\mathbf{R}_{rcm} \in \mathbb{R}^{3\times3}$. As can be seen in Fig. 4, $\mathbf{f}_{ext}$ is then converted into a velocity command $\dot{\mathbf{x}}_{ext}$ with a a min/max saturation function and finally converted into velocity command $\dot{\mathbf{q}}_{d_7}$ by a PD controller.

The micro-scale subsystem is teleoperated using the previously described joystick embedded on the arm terminal body. The position of the joystick $\mathbf{q}_{st} = [\lambda_{st}, k_{st}]^\intercal$ is directly interpreted as the desired joint configuration of the flexible tool as $\mathbf{q}_{d_{tip}}$.

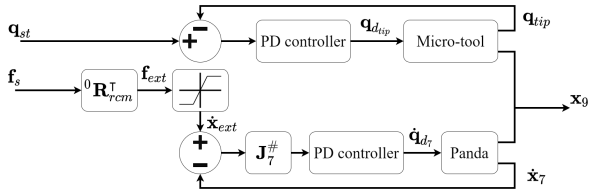

Fig. 4. Control loop architecture of the macro comanipulation and micro tele-operation.

V. EXPERIMENTAL VALIDATION

A. Experimental Setup

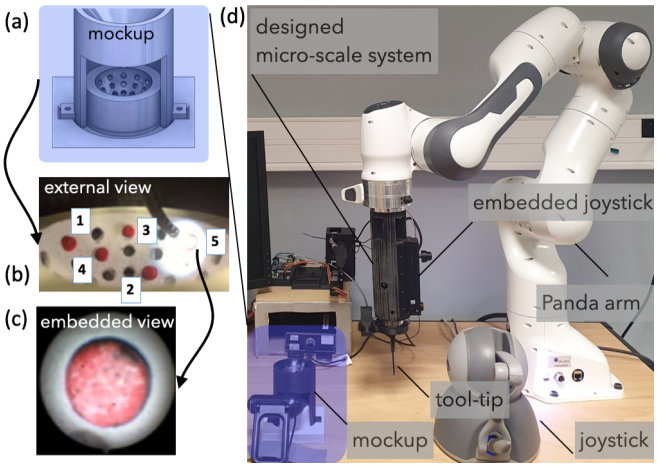

Fig. 5. Experimental setup with (a) the fiberscope integrated visual feedback and (b) the webcam view.

To assess the mechatronic development as well as the proposed controllers, we designed an experimental setup as can shown in Fig. 5. Since this is preliminary work, we have mimicked the cavity of the middle ear, the presence of residual infected tissue, and the surgical procedure. The middle ear cavity is simulated (in scale 1:2) by a mockup with a conic entrance similar to a drilled hole in the mastoid in case of MIS procedure. The residual infected tissues inside the middle ear cavity are mimicked by five targets of 3 mm of diameter placed on a spherical surface (Fig. 5). Two visual feedback are made available to the operator, one via an external webcam (Logitech QuickCam Pro 9000) (Fig. 5(b)) and another from the internal camera that equips the flexible endoscopy system (Fig. 5(c)). The tele-operation mode is performed with the Sensable Phantom OMNI allowing the control of the tool-tip motion. The comanipulation mode is achieved thanks to the F/T sensor attached to the Panda robot end-effector, as well as to an ergonomically designed hand-grip. The remaining 2 DoFs (i.e., the flexible micro-scale system) is controlled using the embedded joystick.

B. Validation Scenario

The carried-out validation scenario consists of pointing, in a given order (here, from 1 to 5), residual infected tissues placed inside a cavity as depicted in Fig. 6(a). The surgeon/operator then has the task of positioning the tool-tip in front of each residual cholesteatoma (i.e., tool-tip oriented as perpendicular as possible to the target). The tool-tip is initially placed in the RCM position, then the operator start controlling the tool-tip inside the cavity passing through the incision and point consecutively the five targets. The operator uses one of the proposed controllers to perform this pointing task. Both the trajectory and the final position of tool-tip are recorded to evaluated the performance of each controller.

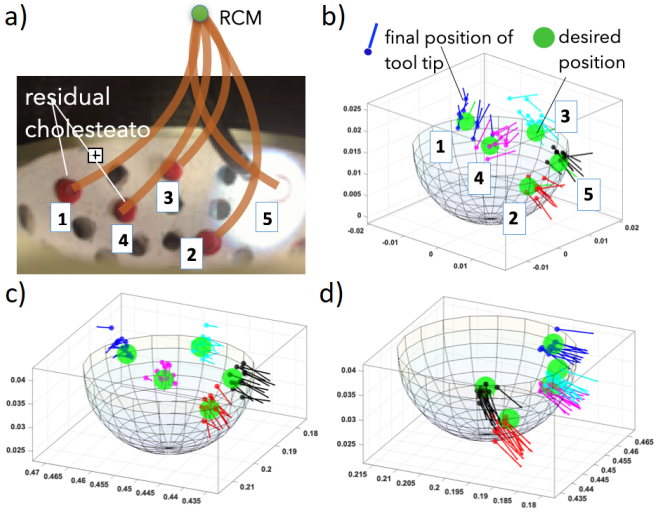

Fig. 6. Plot of the results of the pointing task performed by the recruited volunteers. (a) illustration of the task to be performed manually, (b) manually, (c) using the MCMT method, and (d) using the end-frame tele-operation method. Each volunteer is asked to point (the distal part of the tool-tip must be positioned perpendicular to each target) at the 5 targets (illustrated by a green circle ◯) in a defined order. The final positions of the tool-tip are represented with the symbol —∘.

Note that using the MCMT control mode, the user must be careful not to violate the RCM constraint, while this constraint is automatically fulfilled using the tele-operation mode.

A group of 15 inexperienced subjects (PhD students who are not familiar with tele-operation and comanipulation methods) were recruited. However, each volunteer was given a 10-minutes training session before each test to familiarize them with the experimental setup and each of the developed controllers.

To assess the global performance of the designed dual-scale robotic platform as well as the developed controllers, the Cartesian pose error of the tool tip is recorded when the operator judges that each target (consecutively from 1 to 5) is successfully aimed. The control inputs (velocity, position and force/torque) are recorded in order to monitor the robot behaviour for each performed pointing task. Additionally, the kinematic constraint (RCM) violations are tracked for each volunteer as well as the time required to perform the whole scenario (pointing the five targets). Finally, a comparison of the performance of both control methods is compared to that of a manual mode, which consists of pointing the target manually by holding the fiberscope in the hand while respecting the RCM constraint.

C. Experimental Results

TABLE I

ACCURACY COMPARISON OF THE DIFFERENT CONTROL MODES.

Control mode	Tele-operation	MCMT	Manual
$\bar{e}_x$ (mm)	0.98 ± 0.37	0.83 ± 0.15	1.4 ± 1.00
$\bar{e}_y$ (mm)	1.20 ± 0.28	1.20 ± 0.45	2.3 ± 0.94
$\bar{e}_z$ (mm)	0.95 ± 0.36	1.30 ± 0.10	2.2 ± 1.50
$\bar{e}_{\theta_x}$ (deg)	7.75 ± 1.37	8.54 ± 1.54	13.68 ± 13.88
$\bar{e}_{\theta_y}$ (deg)	4.83 ± 3.40	3.33 ± 1.61	17.68 ± 10.28
$\bar{e}_{\theta_z}$ (deg)	8.97 ± 1.17	9.64 ± 3.53	7.16 ± 4.57
$\bar{e}_{xy}$ (mm)	1.70 ± 0.90	$\mathbf{1.60 \pm 1.10}$	2.90 ± 1.50
$\bar{e}_{\theta_x,\theta_y}$ (deg)	2.92 ± 2.10	$\mathbf{2.46 \pm 1.49}$	20.84 ± 18.92

1) Accuracy: The obtained results for the developed control methods as well as the manual method mode are depicted in Fig. 6. It shown the five targets (represented by a green circle ◯) to be pointed by each volunteer and the final 3D position of the tool-tip when the operator judges that the target is reached (represented by an oriented symbol —∘). Knowing the spatial positions of the desired position of each target as well as the final positions of the tool-tip at the end the pointing task, it is possible to compute the linear and angular accuracy with which each target has been pointed. Thus, the corresponding numerical values for the accuracy evaluation are summarized in Table I and compared to those obtained when the task is performed manually. As mentioned beforehand, the surgical procedure consists of positioning accurately a surgical laser in front of the residual infected tissues to be burned to prevent re-growth of the cholesteatoma. Consequently, the accuracy should be highest on the $x-y$ directions (i.e., the tool should be perpendicular to the $x-y$ plane of the target) without any requirement to touch it. This means that $\bar{e}_z$, and $\bar{e}_{\theta_z}$ can be considered less meaningful than the others Cartesian errors, which explains why the linear and angular errors relative to the z axis are greater than the others.

Based on the Table I, the mean linear error $\bar{e}_x$ and $\bar{e}_y$ are both around 1mm which is in phase with the predefined medical requirements [9], where accuracy must be in the range of one millimeter. Otherwise, it can be highlighted that the manual mode, even if it can be considered accurate for linear motions, it is substantially less accurate for the angular motion compared to both the developed controllers. The mean angular error $\bar{e}_{\theta_x}$ and $\bar{e}_{\theta_y}$ are ~~quite~~ similar for tele-operation and MCMT modes and are estimated to be near 4 degrees, when the manual mode shows an average angular error of about 15 degrees. The first outcome of the evaluation is that the designed dual-scale robotic setup allows improving significantly the accuracy of the positioning task inside the middle-ear cavity, this regardless of the selected control mode (tele-operation or MCMT). Between the MCMT and tele-operation controllers, it turns out that the MCMT method offers a slightly better accuracy. Also, in the survey used in this experiment, the majority of the volunteers stated that the MCMT method is more intuitive and easier to use than the tele-operation mode.

2) Completion time of the pointing task: The required time to achieve the predefined evaluation scenario (i.e., pointing the 5 targets) with the different developed modes was evaluated. It appears that the manual mode is slightly faster ($139.61 \pm 27,66$ seconds) compared to the tele-operation (215.08 ± 114.83 seconds) and MCMT (177.17 ± 49.61 seconds) methods. This may be due to the fact that the initial pose in the case of manual mode is closer to the incision hole comparing to the robotic methods where the initial position is chosen further. Otherwise, when considering only the robotic methods, the MCMT appears to be faster than tele-operation.

3) Respect of the spatial constraint: The last evaluation criterion to evaluate and compare the three modes consists of the number of violations of the RCM constraint which represents a potential risk of collision with the walls of the incision and the facial nerve that may be in the immediate vicinity in some patients. Note the tele-operation mode is not concerned by this evaluation due to the fact that this method does not allow a translational motion of the entering part of the tool-tip at the RCM. An alarm sound was triggered to inform the operator when entering in collision. The MCMT method gives in average 3.7 constraint violations per operator (an average of 0.7 violation per pointing task), when the manual mode scored in average 5.5 constraint violations (an average of 1.1 violations per pointing task).

VI. CONCLUSION

In this paper, a new dual-scale robotic system was designed for middle ear surgery purposes. The developed system consisted of a 7 DoFs collaborative robotic arm on which is fixed 2 DoFs fiberscopic system mimicking a micro-scale robotic system which under development. We have also proposed two control schemes: an end-frame tele-operation method and MCMT approach of the whole redundant kinematic chain.

To assess the performance of the developed robotic setup as well as the controllers, we have implemented an evaluation scenario mimicking the surgical procedure of residual infected tissue ablation with a surgical laser. To do this, a group of 15 volunteers (PhD students who are not familiar with tele-operation and comanipulation methods) was recruited to achieve the demanded task. The designed robotic platform combined with the developed controllers have been shown to meet the requirements of a minimally invasive surgical procedure of the middle ear, especially the MCMT approach, this in terms of accuracy, intuitively, and usability.

The next work will involve the evaluation of the controllers and the robotic platform with a larger number of volunteers including experienced and novice surgeons. We are currently working on an original microrobotic system that will integrate miniature surgical tools, a surgical laser and a fibre-optic camera that will replace the current flexible fiberscope.

REFERENCES

[1] V. Vitiello, S-L. Lee, T. P. Cundy, et al., "Emerging Robotic Platforms for Minimally Invasive Surgery," *IEEE R. in Biomed. Eng.*, vol. 6, pp. 111–126, 2013.

[2] C. L., Kuo, A. S., Shiao, M., et al. "Updates and knowledge gaps in cholesteatoma research," *BioMed Res. Int.*, 2015.

[3] E. L. Derlacki and J. D. Clemis, "Lx congenital cholesteatoma of the middle ear and mastoid," *Annals of ORL*, vol. 74, pp. 706–727, 1965.

[4] P. Bordure, A. Robier, and O. Malard, *Chirurgie otologique et otoneurologique*, Elsevier Masson, 2005.

[5] M. R. Bae, W. S. Kang, and J. W. Chung, "Comparison of the clinical results of attic cholesteatoma treatment: fiberscopic versus microscopic ear surgery," *Clinical and Experimental Otorhinolaryngology*, vol. 12, no. 2, p. 156, 2019.

[6] S. M. Stevens, Z. A. Walters, K. Babo, et al., "Canal reconstruction mastoidectomy: Outcomes comparison following primary versus secondary surgery," *The Laryngoscope*, vol. 129, no. 11, pp. 2580–2587, 2019.

[7] P. Blanco, F. González, J. Holguín, et al., "Surgical management of middle ear cholesteatoma and reconstruction at the same time," *Colombia Médica*, vol. 45, no. 3, pp. 127–131, 2014.

[8] J. E. A. P. d. Aquino, N. A. Cruz Filho, et al., "Epidemiology of middle ear and mastoid cholesteatomas: study of 1146 cases, "*Brazilian J. of Otorhinolaryngology*, vol. 77, no. 3, pp. 341–347, 2011.

[9] B. Dahroug, B. Tamadazte, L. Tavernier, et al., "Review on otological robotic systems: Toward micro-robot assisted cholesteatoma surgery," *IEEE R. in Biomed. Eng.*, vol. 11, pp. 125 - -142, 2018.

[10] B. Dahroug, B. Tamadazte, and N. Andreff. "Unilaterally Constrained Motion of a Curved Surgical Tool." Robotica 38.11: 1940-1962, 2020.

[11] Dahroug, B., Tamadazte, B. and Andreff, N.. "Task Controller for Performing Remote Centre of Motion." Informatics in Control, Automation and Robotics. Springer, Cham, 2018. 117-132.

[12] J.-H. So, B. Tamadazte, and J. Szewczyk, "Micro/macro-scale robotic approach for middle ear surgery," *IEEE T. on Med. Rob. and Bion.*, vol. 2, no. 4, pp. 533–536, 2020.

[13] J.-H. So, S. Sobucki, J. Szewczyk, N. Marturi, and B. Tamadazte, "Shared control schemes for middle ear surgery", Frontiers on Robotics and AI, 2022, (in press).

[14] B. Bell, N. Gerber, T. Williamson, et al., "In vitro accuracy evaluation of image-guided robot system for direct cochlear access," *Otology & Neurotology*, vol. 34, no. 7, pp. 1284–1290, 2013.

[15] M. Miroir, Y. Nguyen, J. Szewczyk, and al., "Design, kinematic optimization, and evaluation of a teleoperated system for middle ear microsurgery," *The Scientific World J.*, 2012.

[16] K. Entsfellner, I. Kuru, G. Strauss, et al., "A new physical temporal bone and middle ear model with complete ossicular chain for simulating surgical procedures," in *IEEE Int. Conf. on Rob. and Biom.*, 2015, pp. 1654–1659.

[17] M. H. Yoo, H. S. Lee, C. J. Yang, et al., "A cadaver study of mastoidectomy using an image-guided human-robot collaborative control system," *Laryngoscope Investigative Otolaryngology*, vol. 2, no. 5, pp. 208–214, 2017.

[18] I. Robert J. Webster and B. A. Jones, "Design and kinematic modeling of constant curvature continuum robots: A review," *The Int. J. of Rob. Res.*, vol. 29, no. 13, pp. 1661–1683, 2010.

[19] F. Nageotte, P. Zanne, and M. D. Mathelin, "Robotic Assistance to Flexible Endoscopy by Physiological Motion Rejection, *IEEE T. on Rob.*, 27 (2), pp.346-359, 2011.

[20] A. Simorov, R. S. Otte, C. M. Kopietz, et al., "Review of surgical robotics user interface: what is the best way to control robotic surgery?" *Surgical endoscopy*, vol. 26, pp. 2117–25, 2012.

[21] M. Adjigble, N. Marturi, V. Ortenzi and R. Stolkin, "An assisted telemanipulation approach: combining autonomous grasp planning with haptic cues," *IEEE/RSJ Int. Conf. on Intel. Rob. and Sys.*, 2019, pp. 3164-3171.

[22] J. Colan, J. Nakanishi, T. Aoyama, et al., "A cooperative human-robot interface for constrained manipulation in robot-assisted endonasal surgery" *Applied Sciences*, vol. 10 (14), 2020.